https://doi.org/10.5194/essd-2024-170
Preprint. Discussion started: 15 May 2024

Open Access Earth System Science Data Discussions

Retrieving Ground-Level $PM_{2.5}$ Concentrations in China (2013-2021) with a Numerical Model-Informed Testbed to Mitigate Sample Imbalance-Induced Biases

Siwei Li [1,3,4], Yu Ding[1], Jia Xing[2], Joshua S. Fu[2]

[1]Hubei Key Laboratory of Quantitative Remote Sensing of Land and Atmosphere, School of Remote Sensing and Information Engineering, Wuhan University, Hubei, 430000, China
[2]Department of Civil and Environmental Engineering, the University of Tennessee, Knoxville, TN 37996, USA
[3]State Key Laboratory of Information Engineering in Surveying, Mapping and Remote Sensing, Wuhan University, Wuhan 430079, China
[4] Hubei Luojia Laboratory, Wuhan University, Wuhan 430079, China

Correspondence to: Siwei Li (siwei.li@whu.edu.cn); Jia Xing (jxing3@utk.edu)

Abstract. Ground-level $PM_{2.5}$ data derived from satellites with machine learning are crucial for health and climate assessments, however, uncertainties persist due to the absence of spatially covered observations. To address this, we propose a novel testbed using untraditional numerical simulations to evaluate $PM_{2.5}$ estimation across the entire spatial domain. The testbed emulates the general machine-learning approach, by training the model with grids corresponding to ground monitor sites and subsequently testing its predictive accuracy for other locations. Our approach enables comprehensive evaluation of various machine-learning methods' performance in estimating $PM_{2.5}$ across the spatial domain for the first time. Unexpected results are shown in the application in China, with larger $PM_{2.5}$ biases found in densely populated regions with abundant ground observations across all benchmark models, challenging conventional expectations and are not explored in the recent literature. The imbalance in training samples, mostly from urban areas with high emissions, is the main reason, leading to significant overestimation due to the lack of monitors in downwind areas where $PM_{2.5}$ is transported from urban areas with varying vertical profiles. Our proposed testbed also provides an efficient strategy for optimizing model structure or training samples to enhance satellite-retrieval model performance. Integration of spatiotemporal features, especially with CNN-based deep-learning approaches like the ResNet model, successfully mitigates $PM_{2.5}$ overestimation (by 5-30 μg m^{-3}) and corresponding exposure (by 3 million people • μg m^{-3}) in the downwind area over the past nine years (2013-2021) compared to the traditional approach. Furthermore, the incorporation of 600 strategically positioned ground-measurement sites identified through the testbed is essential to achieve a more balanced distribution of training samples, thereby ensuring precise $PM_{2.5}$ estimation and facilitating the assessment of associated impacts in China. In addition to presenting the retrieved surface $PM_{2.5}$ concentrations in China from 2013 to 2021, this study provides a testbed dataset derived from physical modeling simulations which can serve to evaluate the performance of data-driven methodologies, such as machine learning, in estimating spatial $PM_{2.5}$ concentrations for the community.

https://doi.org/10.5194/essd-2024-170
Preprint. Discussion started: 15 May 2024

1 Introduction

Accurate knowledge of $PM_{2.5}$ pollution is vital for understanding its impact on human health (Lelieveld et al., 2015; Geng et al., 2021) and the climate (Mitchell et al., 1995; Bellouin et al., 2005). Satellite products provide direct measurements of aerosol loading on broad spatial and temporal scales. While, the Aerosol Optical Depth (AOD) measured by satellites reflects the total column of particular matters, challenged by the complex relationship between AOD with ground $PM_{2.5}$ influenced by various factors (Hoff et al., 2009), including aerosol chemical composition and vertical profiles. Compared to traditional statistics, machine learning excels in addressing non-linearities. Therefore, numerous recent studies leverage machine learning, such as Random Forest (RF) (Hu et al., 2017), XGBoost (Xiao et al., 2018), lightGBM (Zhong et al., 2021), and deep learning models (Li et al., 2020; Yan et al., 2020; Wang et al., 2022a; Wang et al., 2022b; Wei et al., 2023) to establish correlations between AOD and $PM_{2.5}$, treating AOD and related factors, including meteorological variables, as features to predict surface $PM_{2.5}$ based on ground measurements (Ma et al., 2022). However, a limitation arises as most ground measurements are concentrated in urban and polluted areas. Their main purpose is to monitor the high pollution level to protect human health, leading to an uneven spatial distribution. It is expected that training models predominantly on urban sites introduce an imbalance in ground-based measurements, resulting in significant uncertainties in spatially allocating surface $PM_{2.5}$ based on satellite AOD (Shin et al., 2020). This deficiency might be particularly notable in suburban areas experiencing downwind transport of $PM_{2.5}$ from urban areas (Bai et al., 2022). Moreover, despite the widespread global use of satellite-retrieved surface $PM_{2.5}$ products, no ground truth is available for evaluating performance in the machine-learning interpolations for suburban/rural areas along pollutant transport pathways. Consequently, uncertainties in $PM_{2.5}$ estimation for these areas remain unexplored, and solutions to reduce such uncertainties are yet to be developed.

To overcome these limitations, we introduce a novel testbed utilizing a numerical model, specifically a chemical transport model (CTM) such as the Community Multiscale Air Quality Modeling System developed by the U.S. EPA and its community (Appel et al., 2013), to establish ground-truth data beyond monitor points. This allows for the evaluation of interpolation performance using various machine-learning models and provides solutions to mitigate the uncertainties stemming from the sample imbalance problem. More specifically, we emulate traditional machine-learning methods but by using CTM-simulated $PM_{2.5}$ concentrations in grid cells corresponding to ground monitor sites as labels for training machine-learning models. Subsequently, we validate the trained model's performance in predicting $PM_{2.5}$ concentrations in other grid cells. In addition to providing a "ground-truth" for assessing performance across the entire space, the CTM simulated data acts as a testbed for efficiently seeking solutions to enhance satellite-retrieval model performance. This involves optimizing features, model structure, and training samples, as depicted in Figure 1.

The proposed testbed is implemented in a China domain, utilizing one whole year simulation of 2017 with a 27km by 27km resolution. To ensure internal consistency during training, all the feature and label data are derived from the input and output of a commonly used CMAQ. The meteorological variables include U-wind, V-wind, humidity, 2-meter temperature, convective velocity scale, short-wave radiation, 10-meter wind speed, PBL height, leaf-area-index (LAI), cloud fraction, and

https://doi.org/10.5194/essd-2024-170
Preprint. Discussion started: 15 May 2024

precipitation, simulated by the Weather Research & Forecasting Model (WRF) (Skamarock et al., 2008). The simulated Aerosol Optical Depth (AOD) is calculated based on simulated $PM_{2.5}$ chemical compositions and corresponding meteorological variables across all vertical layers (Liu et al., 2010). We also include the NO_2 column density as an important feature as it is highly correlated with emission sources and can be directly observed from satellites to better represent the emission information (Martin et al., 2003). Similarly, the simulated NO_2 column density is calculated based on simulated NO_2 concentrations and corresponding meteorological variables across all vertical layers.

In addition, we conduct model training using nine-year observational data from 2013 to 2021 to evaluate potential biases under real-world conditions. This is quantified by measuring the difference in retrieved $PM_{2.5}$ between the traditional model and the improved retrieval method optimized with the proposed testbed. The dataset for this evaluation comprises the Moderate Resolution Imaging Spectroradiometer (MODIS) (Remer et al., 2008) satellite observations for AOD, Ozone Monitoring Instrument (OMI) (Celarier et al., 2008) satellite data for NO_2 column density, and ground monitor observations of $PM_{2.5}$ from the China National Environmental Monitoring Center (CNEMC, coving more than 600 grid cells of 27km by 27km in total) (Kong et al., 2021).

2 Methods

2.1 Numerical model WRF/CMAQ

In this study, we utilized version 5.2 of the Community Multiscale Air Quality (CMAQ) model (Appel et al., 2018), incorporating the Carbon Bond 6 (Yarwood et al., 2010) gas-phase chemistry mechanism and the AERO6 particulate matter chemistry mechanism. CMAQ, a widely recognized CTM, is renowned for its accurate simulation of air pollutant concentrations, including $PM_{2.5}$, attributed to its comprehensive representation of particulate matter formations. Meteorological data were generated using the Weather Research and Forecasting (WRF) model, version 3.8, configured in the same manner as our previous studies (Ding et al., 2019ab). Emission data were obtained from the high-resolution emission inventory developed by Tsinghua University (ABaCAS-EI) (Zheng et al., 2019), characterized by a spatial resolution as fine as 1km-by-1km and a temporal resolution of 1 hour. Biogenic emissions were derived from the estimation of the Model for Emissions of Gases and Aerosols from Nature (MEGAN) (Guenther et al., 2012). We conducted a thorough assessment of the performance of WRF and CMAQ in simulating meteorological variables and air pollutant concentrations, employing extensive comparisons with observational data in our previous studies (Ding et al., 2019ab).

The simulation domain spans a significant portion of East Asia and is depicted by a grid consisting of 182 rows and 232 columns, featuring a horizontal resolution of 27 km by 27 km. The entirety of the troposphere (from ground level to 100mb) is represented using 14 layers with sigma values, namely 1.00, 0.995, 0.99, 0.98, 0.96, 0.94, 0.91, 0.86, 0.8, 0.74, 0.65, 0.55, 0.4, 0.2, and 0.00. These sigma values correspond to altitudes of 19, 57, 114, 230, 386, 584, 910, 1375, 1908, 2618, 3598, 5061, 7620, and 11944 meters above the ground level, both at the domain and on an annual averaged basis.

https://doi.org/10.5194/essd-2024-170
Preprint. Discussion started: 15 May 2024

We align the simulated $PM_{2.5}$ concentrations from CMAQ with the CNEMC based on their respective locations, treating them as the "label" for training the machine-learning model. The remaining grid cells encompass the surrounding $PM_{2.5}$, which has not been previously evaluated in other studies. This paper focuses on assessing the model's performance in predicting these points, accounting for over 90% of the total grid cells. The simulation data serves as the "ground truth" for the evaluation the output of the machine-learning model.

2.2 Decision tree-based machine learning method

This study employed three decision-tree-based machine learning algorithms, namely Random Forest (Belgiu and Drăguţ, 2016), XGBoost (Chen and Guestrin, 2016), and LightGBM (Ke et al., 2017), to serve as benchmark cases, given their widespread use in previous studies. Additionally, Deep-RF (Zheng et al., 2021), known for its superior performance (Wei et al., 2023), was included as an additional method to be evaluated in this study.

We incorporated similar features used in the machine-learning model, including observed meteorological variables (WRF output) and land use information. The reason is we deliberately avoided using CTM simulation results for two key reasons, while some previous studies included CTM modeling results as additional features in training machine learning models. First, the CTM will be applied to the testbed to evaluate the model's performance, and introducing CTM results could leak information as these results are utilized as labels and therefore cannot be used as input thereafter. Second, we aimed to propose a comprehensive CTM-free method that relies exclusively on satellite products and meteorological variations obtained from observations. This choice is motivated by the low efficiency of conducting CTM and the uncertainties it introduces. Furthermore, the only additional information provided by the CTM is related to emissions, which still suffers from uncertainties. Therefore, instead of relying on CTM or prior emission data, we introduce the NO_2 column density. This variable is highly correlated with emission sources and can be directly observed from satellites, offering a more accurate representation of emission information.

Given our objective to assess grid cells outside the designated "label", there is no overlap between the training and test datasets. To evaluate the model's performance on the labels, we employ temporal validation. Specifically, the model is trained using data from only the first 25 days of each month, and the remaining days are reserved for testing. This approach helps gauge the model's effectiveness in handling temporal variations and provides a robust assessment of its performance on the specified labels.

2.3 Residual neural network method (ResNet)

The incorporation of spatiotemporal-neighborhood features is crucial for enhancing the model's capability to discern the evolution of vertical profiles in both urban and downwind areas (Chen et al., 2023). Beyond simply including corresponding features from the surrounding neighborhood grid cells as additional predictors for predicting $PM_{2.5}$ concentration at the target grid cells in decision tree-based methods, we also employ a deep-learning method, which is ResNet (He et al., 2016). This

https://doi.org/10.5194/essd-2024-170
Preprint. Discussion started: 15 May 2024

choice is motivated by its demonstrated advantage in handling the nonlinearity inherent in atmospheric processes, as suggested in our previous study (Xing et al., 2020).

The ResNet consists of an initial layer with 128 channels and incorporates 8 residual blocks. The feature maps, encompassing meteorological variables, land use information, and AOD, are fed into the Conventional Neural Network (CNN)-based structure with a 3 by 3 kernel size, as illustrated in Figure S1. Additionally, we also incorporate the feature in the previous and next day as additional features to help capture the transport flow of pollutants in the model. The training loss will concentrate solely on points corresponding to the monitor sites, generating predictions exclusively for these specific locations, given the scattered nature of the labels. As a result, predictions for other points will be entirely out-of-sample, relying on data from the same locations as the monitor sites.

Throughout the training phase, we employed the Mean Squared Error (MSE) loss function, conducting a total of 1000 epochs, which demonstrated sufficient effectiveness in achieving robust performance during both training and testing. The learning rate started at 0.0001 and underwent linear decay, reaching zero by the conclusion of the training process. Additionally, we utilized the Adam optimizer (Kingma and Ba, 2014) to enhance the convergence of the model.

3 Results

3.1 Imbalance in site distribution leads traditional methods to overestimate downwind $PM_{2.5}$

To explore uncertainties in traditional machine-learning methods, we initially adhere to their typical design, relying exclusively on local features within each grid cell. This approach involves utilizing only the feature data from the same location as the target grid cell. The trained model with the Random Forest method (RF) successfully captures the spatial distribution of $PM_{2.5}$, showing elevated levels in east China and lower levels in the west (Figure 2a). It exhibits acceptable performance for the "label" grid cells during validation (Figure 2b, R^2=0.98 and RMSE=5.28 μg m^{-3} in the training dataset, and R^2=0.81 and RMSE=16.1 μg m^{-3} in the test dataset).

However, considerable errors are observed across space, particularly in polluted regions with high baseline $PM_{2.5}$ concentrations (Figure 2c). Positive biases (i.e., predictions greater than CMAQ) increase with the distance from monitor sites, even as $PM_{2.5}$ concentrations decrease. This suggests an overestimation in predictions for downwind areas away from the monitor sites (Figure 2d). This is mainly attributed to the traditional model's difficulty in discerning variations in vertical profiles between urban and suburban areas. Training is primarily focused on urban areas, where pollution is concentrated near the surface due to ground-level emission sources. In contrast, pollution in downwind areas is transported aloft. Therefore, the model, trained with urban sites, attributes more pollution to the ground level from the AOD, leading to overestimation in downwind areas (as illustrated in Figure 2e).

Contrary to traditional expectations, significant errors occur mostly in East China rather than in the West. While the east has more densely located monitor sites, they are primarily situated in urban centers. This imbalance in site distribution, combined with much higher concentrations, results in substantial biases in east China.

https://doi.org/10.5194/essd-2024-170
Preprint. Discussion started: 15 May 2024

Similar phenomena are observed in three other benchmark models that have been applied in previous studies, specifically XgBoost, LightGBM, and the deep-RF. All of these models demonstrate robust performance in both training and testing at the monitor sites (R^2>0.8 and RMSE<16.2 μg m^{-3} in the test cases, as depicted in Figure S2). However, they display similar uncertainties in downwind $PM_{2.5}$, with significant errors occurring in the surrounding grid cells of the monitor sites rather than in remote sites where concentrations are relatively low. Clearly, we can conclude that the uneven distribution of sites introduces considerable biases in $PM_{2.5}$ estimation within traditional methods that rely on local features.

3.2 Inclusion of spatiotemporal-neighbourhood features improves surrounding $PM_{2.5}$ prediction other than traditional approaches

As previously discussed, the ineffectiveness of a machine-learning model trained on imbalanced samples can be attributed primarily to insufficient information regarding the spatial variation of vertical profiles from the source to the downwind area. To enhance the integration of crucial information regarding vertical profiles, we introduce spatiotemporal-neighbourhood features into the model. This addition aims to empower the model with the capability to distinguish between urban and downwind areas. Leveraging the convolutional neural network (CNN) -based structure, known for its effectiveness in exploring non-linear relationships among neighbouring grid cells, we opt for the widely used deep-learning model ResNet. This choice facilitates the establishment of non-linear relationships between predicted $PM_{2.5}$ concentrations and multiple spatiotemporal-neighbourhood features. In contrast to traditional methods that solely focus on single-time features, our approach incorporates both preceding and succeeding time features to enhance the model's capacity to discern differences among urban and downwind grid cells. This inclusion is motivated by the fact that plume transport is predominantly influenced by flow dynamics, represented by the variation in the temporal neighbourhood (before and after) features. Our previous studies have also demonstrated the effectiveness of linking grid cells with time-series information in $PM_{2.5}$ estimation, underscoring the rationale for this inclusive approach (Teng et al., 2023; Ding et al., 2024). Additionally, considering that AOD measured by satellites, such as MODIS, captures only a single time step while predictions are made for daily averages, the inclusion of extra time-step information proves beneficial in capturing a broader temporal context compared to a single time snapshot (the model noted as ResNet-time).

The results indicate that while the spatial pattern of $PM_{2.5}$ predicted with ResNet closely resembles that of other models (Figure 3a), it significantly enhances model performance in predicting $PM_{2.5}$ for both the training dataset (reducing RMSE from 4 to 2 μg m^{-3} and increasing R^2 slightly) and the test dataset (reducing RMSE from 14 to 8 μg m^{-3} and increasing R^2 from 0.8 to 0.9). This improvement can be attributed to the incorporation of both spatial and temporal features. The performance of the traditional RF model is enhanced by replacing it with the ResNet model, and this improvement is further amplified by including temporal features (previous and next-time steps) in the ResNet-time model (see Figure 3b). The incorporation of surrounding features in the ResNet-time model significantly mitigates errors in East China across the spatial domain (see Figure 3c). However, some deterioration is observed in the West, primarily attributable to limited samples. The model, becoming more complex, lacks sufficient training samples in the West, leading to overfitting in that region.

https://doi.org/10.5194/essd-2024-170
Preprint. Discussion started: 15 May 2024

The inclusion of spatiotemporal-neighborhood features also significantly improves the performance of traditional benchmark models, by incorporating corresponding features of the surrounding eight neighborhood grid cells and the temporal neighbourhood (before and after) information as additional predictors for predicting $PM_{2.5}$ concentration at the target grid cells. Improvements are observed in both training and test datasets across all four benchmark models, as depicted in Figure S3. Notably, all models demonstrate a reduction in RMSE after integrating spatiotemporal-neighborhood features, especially for the downwind area (within the distance of 1-3 grid cells) (see Figure 3d). However, performance is barely improved or even worsens in faraway sites (distance >4 grid cells) due to the limitations in training samples. Clearly, enhancing the training sample is crucial for further improving the model predictions, as discussed in the following.

3.3 Balancing site distribution is crucial to improve the prediction for the entire space of $PM_{2.5}$

Utilizing the ResNet-time model, we explore the correlation between model errors and the distance to monitor sites, as well as the concentrations at the nearest monitor. Notably, significant errors were observed in sites within a two-grid-cell distance (refer to Figure S4) and those near monitors exhibiting high concentrations (refer to Figure S5). Consequently, two criteria, namely 1) the baseline concentration in nearby monitor sites (referred to as B-conc); 2) the distance from monitor sites (referred to as D-site), are established to select the potential samples to refine predictions across the spatial domain.

Three sample groups are delineated based on the criteria:

(1) B-conc >30 μg m^{-3}, D-site: 1-5 grid-cell distance;

(2) B-conc within 20-30 μg m^{-3}, D-site: 2-5 grid-cell distance;

(3) B-conc within 10-20 μg m^{-3}, D-site: 3-5 grid-cell distance.

This design not only focused on the area suffering large impacts on pollution but also allowed the selection of sites in remote regions with moderate baseline concentrations, as illustrated in Figure S6. To enhance the representativeness of the chosen sites, random selections are independently conducted within each of the three groups, encompassing 10% (~300 sites, half of the existing sites), 20% (~600 sites, equal to the existing sites), 30% (~900 sites, 1.5 times the existing sites), 40% (~1200 sites), 70% (~2100 sites), and all samples (~3000 sites). The testbed developed in this study enables an efficient evaluation of the model's performance by training it with these additional sites.

The results indicate that an increase in training samples effectively enhances the model's performance in $PM_{2.5}$ estimation, with RMSE continuously decreasing as the number of samples increases (see Figure 4a). This improvement is primarily observed in the downwind area, while the performance at monitor sites deteriorates due to the original model being overfitted to these specific sites. The rate of improvement diminishes after the inclusion of 20% of samples, implying that just doubling the current ground monitors wisely can effectively balance the training samples to ensure the accuracy of $PM_{2.5}$ estimations (RMSE reduced by 20-30%). As illustrated in the example with 20% sample inclusion in Figure 4b, it is recommended that more than half of the new sites be set up in eastern China, where $PM_{2.5}$ concentration is high. Additionally, 10% of the sites are suggested to be established in remote areas that are influenced by transport from heavy pollution regions but lack nearby ground measurements. The inclusion of additional sites proves effective in significantly

https://doi.org/10.5194/essd-2024-170
Preprint. Discussion started: 15 May 2024

reducing prediction errors across the entire spatial domain, leading to a much closer agreement with the ground-truth (Figure 2a) in the $PM_{2.5}$ spatial pattern.

It is important to acknowledge that errors may be influenced by factors beyond site distribution problems, such as systematic errors arising from insufficient features. Baseline errors are referenced to those trained with all points using ResNet, amounting to within 1.7 μg m^{-3} (Figure S7). Similarly, training with all points may increase errors in monitor sites, as the original model might be overfitted to these sites rather than representing the overall situation (Figure 4a).

3.4 Potential biases and optimized site selections under real-world conditions

While ground measurements are unavailable for the entire space, we conducted the evaluation using both the traditional RF method and the ResNet-time model developed previously with satellite data. Both models were trained using real-world satellite data and ground monitor $PM_{2.5}$ observations during 2013-2021, and their differences can be considered as part of the potential biases, associated with the influence of incorporating spatiotemporal features for enhancing the model's ability in identifying vertical structure.

The results suggest that both models effectively replicate the time series of monthly mean $PM_{2.5}$ concentrations across monitor sites from 2013 to 2021 (see Figure 5a). However, considerable disparities emerge in their predictions for other areas. The new predictions using the ResNet-time model generally exhibit lower $PM_{2.5}$ concentrations, particularly in the north and west regions (Figure 5b), with a more significant impact observed as the distance to ground monitor sites increases (Figure 5c). A notable discrepancy in population-weighted $PM_{2.5}$ concentration is observed in East China which has a large population, implying that the errors also applied in human health assessment. Since the ResNet-time model demonstrates superior performance compared to the traditional RF model in both training (reducing RMSE from 6 to 2.5 μg m^{-3} and increasing R^2 from 0.9 to 1.0) and test data (reducing RMSE from 20 to 15 μg m^{-3} and increasing R^2 from 0.4 to 0.6), it appears that traditional methods might significantly overestimate $PM_{2.5}$ concentrations (by 5-30 μg m^{-3}) and $PM_{2.5}$ exposure in suburban/rural areas by 3 million people • μg m^{-3} (Figure 5c) due to the sample imbalance problem throughout 2013-2021. Similar results are also suggested in the other three benchmark models (Figure S8-S9). The actual errors might be even larger, as the inclusion of spatiotemporal-neighbourhood features in the ResNet-time model can only mitigate a portion of the errors.

Incorporating a significant number of additional sites is necessary to balance the training samples and further reduce the uncertainties. Following the two previously defined criteria (i.e., B-conc and D-site), three groups of samples are selected. Similarly, 20% of samples (631 in total, close to the number of existing sites) in each group are proposed as potential additional sites in the future, as presented in Figure 5d. Group 1 (30% of the total add-on sites) is primarily situated in polluted regions (B-conc > 60 μg m^{-3}, D-site: 1-5 grid-cell distance), encompassing areas such as the Beijing-Tianjin-Hebei region and the desert region in the west. Group 2 (40% of the total add-on sites) represents sites with a moderate distance to existing monitor sites with a heavier pollution level, compared to Group 1 (B-conc within 40-60 μg m^{-3}, D-site: 2-5 grid-cell distance). Lastly, Group 3 (30% of the total add-on sites) represents sites located far away from existing monitor sites with a

https://doi.org/10.5194/essd-2024-170
Preprint. Discussion started: 15 May 2024

low pollution level (B-conc < 40 μg m^{-3}, D-site: 4-5 grid-cell distance), situated in remote areas with limited influence from transport originating in pollution regions. As indicated by the previous testbed analysis, including these additional sites has the potential to reduce errors by at least 20%, leading to a more accurate machine-learning estimation of $PM_{2.5}$ concentrations with a more balanced training sample set.

4 Data availability

The Numerical Model-Informed Testbed and corresponding estimated PM2.5 concentrations spanning the past nine years (2013-2021) can be found at https://doi.org/10.5281/zenodo.11122294 (Li et al., 2024)

5 Code availability

The ResNet-time model developed in this study can be downloaded at https://doi.org/10.5281/zenodo.11122294 (Li et al., 2024).

6 Discussion and Conclusions

Amidst the advancements in satellite products and machine learning techniques, ground-level $PM_{2.5}$ data has found extensive applications in health assessments and related fields. However, its uncertainties have remained unexplored due to the lack of ground-truth data covering the whole space. This study designed a physically-informed testbed by leveraging the CTM simulations to evaluate PM2.5 estimation across the entire spatial domain, quantified the associated uncertainties in the $PM_{2.5}$ mapping across the whole space. Traditionally, it was believed that errors would be significant in remote areas with few or no ground-based measurements, while observation-dense regions, following the spatial interpolation principle, were expected to exhibit better accuracy. Contrary to expectations, our findings reveal that the largest uncertainties occur differently. One reason is the heavier baseline $PM_{2.5}$ concentration, and another significant factor is the sample training imbalance problem. Ground-based measurements, designed for monitoring heavy pollution, are predominantly located in urban or industrial areas. Using these measurements as training samples misleads the machine learning model into assuming uniform similarity to urban sites, especially in vertical structures. In reality, the vertical profile varies significantly with the flow after the pollutant is emitted from the source. This sample imbalance issue causes the machine-learning model to fail in providing accurate predictions for $PM_{2.5}$ across the entire spatial domain.

The newly developed testbed also enables us to seek best solution, such as optimizing model structure or enhancing training samples, to improve satellite-retrieval model performance. Our results underscore the importance of incorporating spatiotemporal features to enhance the machine learning model's ability to identify differences among urban and downwind conditions that are not explored in the recent literature. However, fully addressing the sample imbalance problem

https://doi.org/10.5194/essd-2024-170
Preprint. Discussion started: 15 May 2024

necessitates the addition of more ground-measurement sites to achieve a more balanced distribution of training samples for machine learning in China. In recent years, the Chinese government has expanded monitor sites towards suburban areas, increasing the total monitor sites by about 400 (from about 1600 in 2017 to about 2020 in 2021). While these additional samples have effectively improved $PM_{2.5}$ predictions (as presented in Figure S10), they account for only about 100 grid cells in the 27km by 27km domain. According to estimations in this study, approximately 600 grid cells are needed to locate monitor sites in the future.

This study also successfully demonstrates leveraging the CTM model to generate abundant data for testing machine-learning methods, overcoming limitations associated with data availability. While derived from a numerical model-based testbed, it is important to acknowledge that the numerical model itself may encounter uncertainties related to emissions and chemical mechanisms, potentially leading to discrepancies with real observations. Nevertheless, the testbed serves as a specific scenario for evaluating satellite-retrieval methods, with the expectation that these methods should perform effectively in various scenarios, including those generated from CTM simulations. Therefore, the errors observed in the CTM-based testbed also imply their existence when applied to real data. Additionally, although this study primarily focuses on the analysis of $PM_{2.5}$ in China, the identified errors may extend to other pollutants and countries as a whole, particularly when facing similar sample-imbalanced problems (i.e., lacking suburban or rural representative sites). Leveraging the testbed developed in this study can be immensely helpful in examining uncertainties in other pollutants and countries, or other geoscience applications facing similar sample imbalance challenges.

Author contributions

SL and JX designed the experiments and carried them out. YD helped with the data processing. JF helped with the manuscript review. SL prepared the manuscript with contributions from all co-authors.

Competing interests

The authors declare that they have no conflict of interest.

Acknowledgements

This work was supported by the Open Research Program of the International Research Center of Big Data for Sustainable Development Goals (CBAS2022ORP01), and Microsoft Climate Research Initiative program.

https://doi.org/10.5194/essd-2024-170
Preprint. Discussion started: 15 May 2024

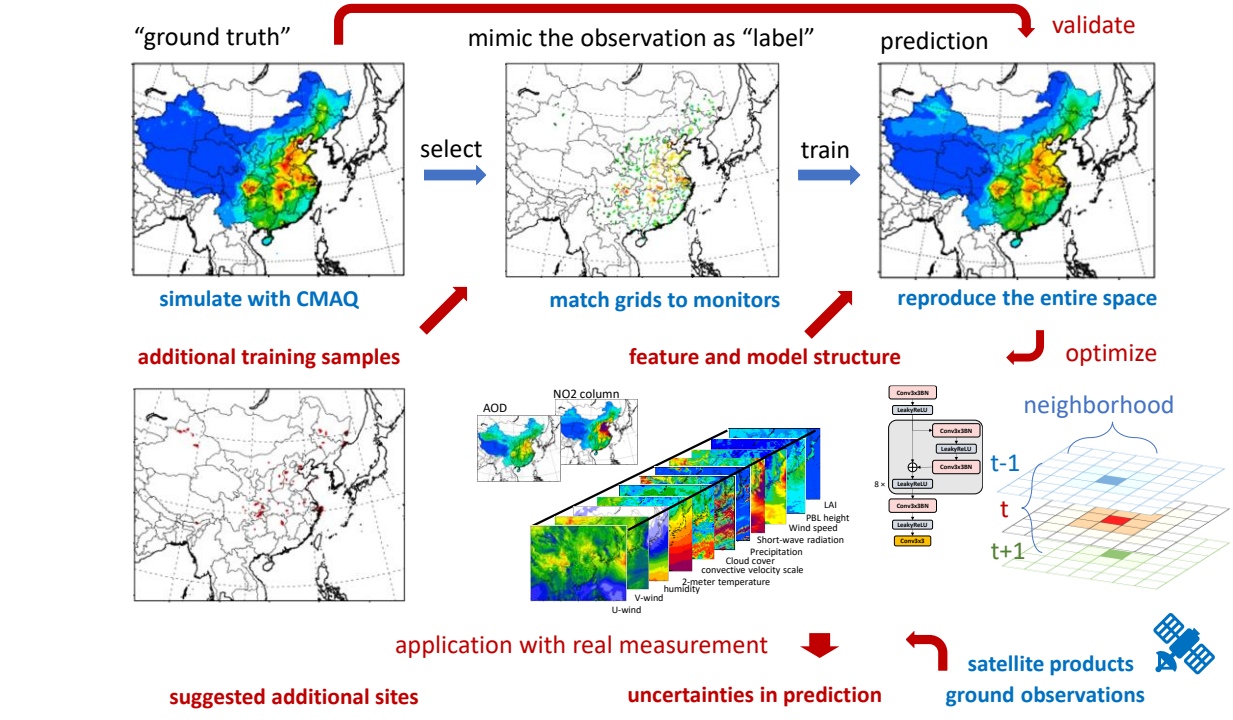

Figure 1: The proposed testbed for evaluation of satellite-retrieving surface $PM_{2.5}$ concentration

https://doi.org/10.5194/essd-2024-170
Preprint. Discussion started: 15 May 2024

Open Access Earth System Science Data Discussions

320

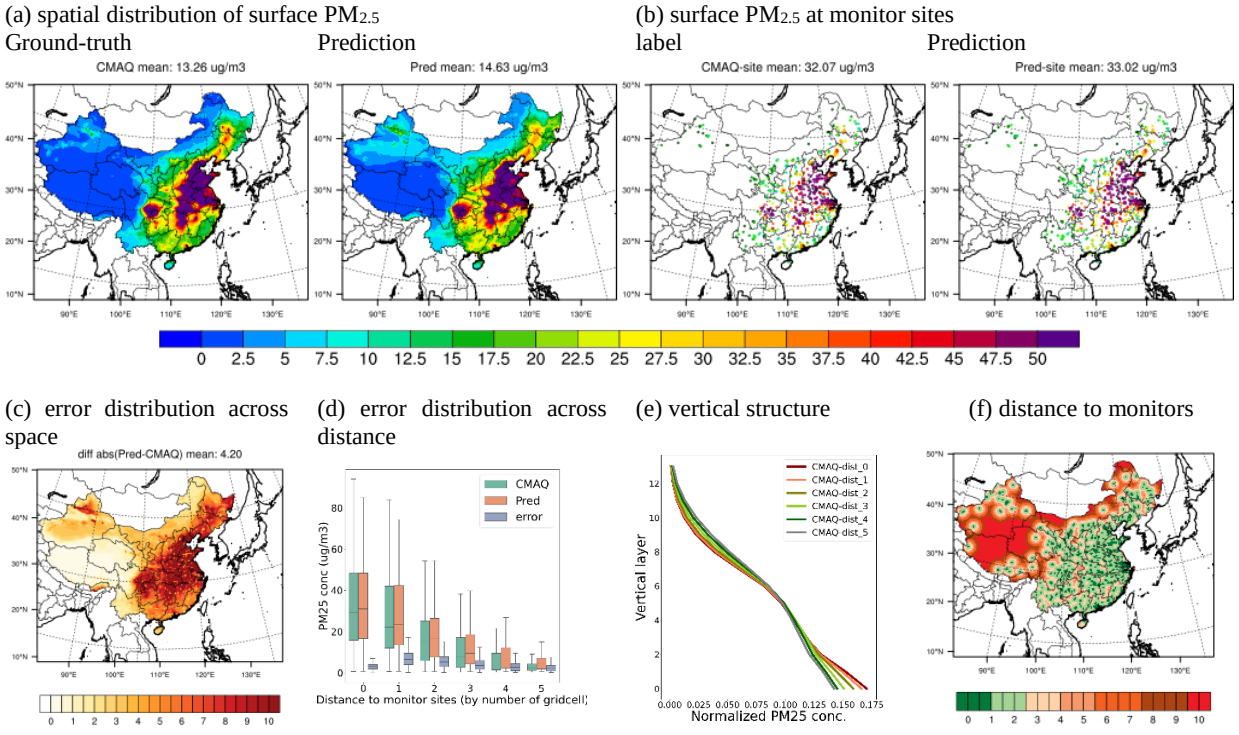

Figure 2: Performance in predicting surface $PM_{2.5}$ with monitor-located Random Forecast model

https://doi.org/10.5194/essd-2024-170
Preprint. Discussion started: 15 May 2024

Open Access Earth System Science Data Discussions

325

(a) Prediction

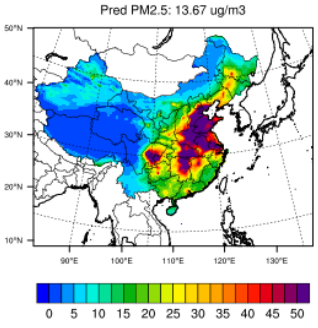

(b) Performance on the sites

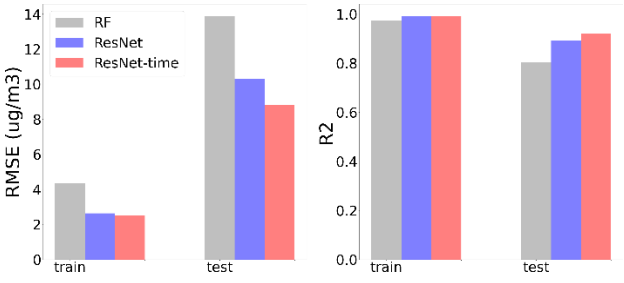

(c) difference in errors*

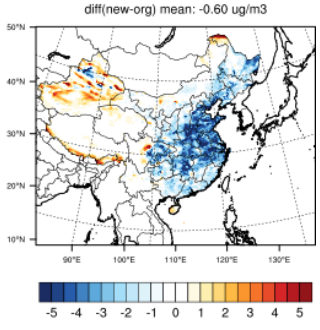

(d) difference in errors across distance to monitors**

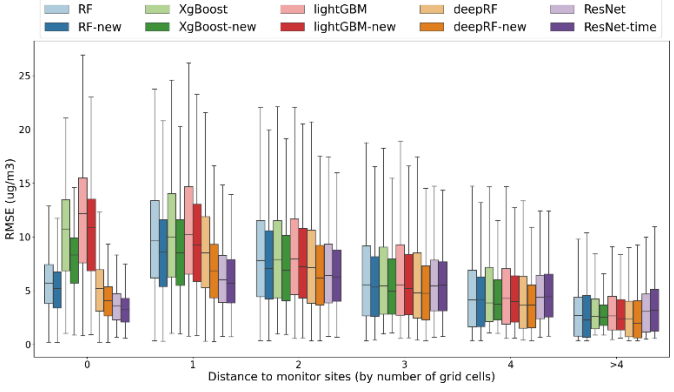

Note: * blue: better; red: worse; **-new: add surrounding features into the prediction in each model

Figure 3: Improvement after implementing the features in surrounding grid cells with ResNet (compared to RF in b and c, compared to all models in d)

https://doi.org/10.5194/essd-2024-170
Preprint. Discussion started: 15 May 2024

Open Access Earth System Science Data Discussions

330

(a) performance in scenarios with adding points

overall domain

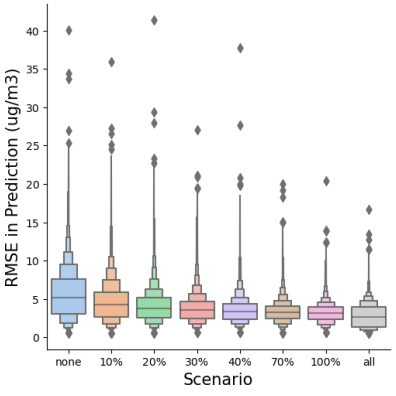

across distance to monitor sites

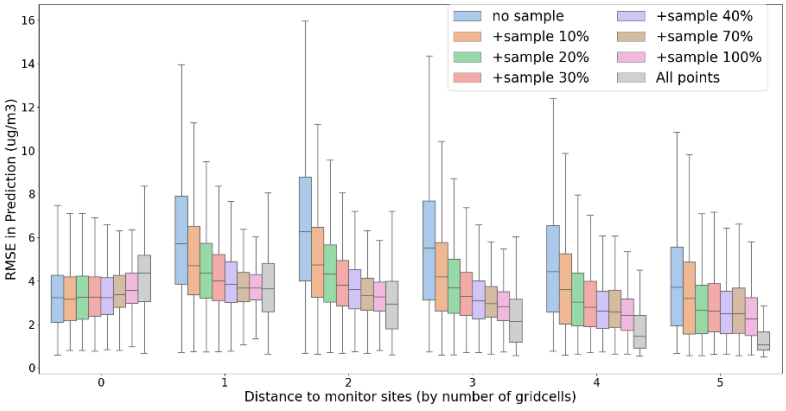

(b) +sample 20%

Location of sites

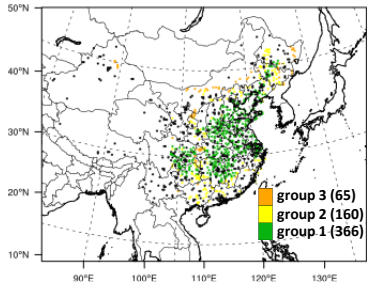

*black dot: original monitor sites (619)

Prediction

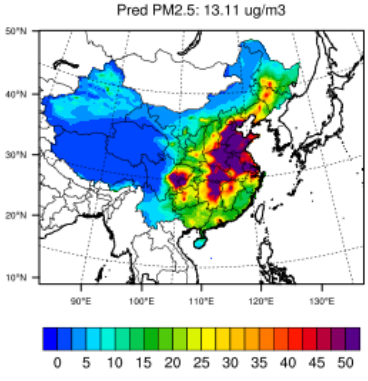

difference in errors

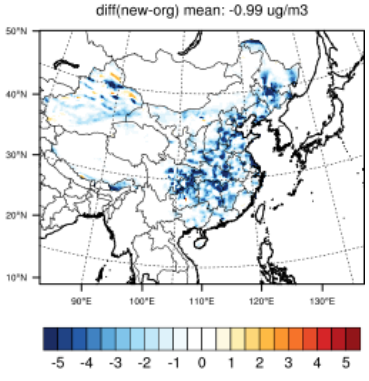

Figure 4: Improved Performance through Integration of Additional Sites with ResNet Model

https://doi.org/10.5194/essd-2024-170
Preprint. Discussion started: 15 May 2024

Open Access Earth System Science Data Discussions

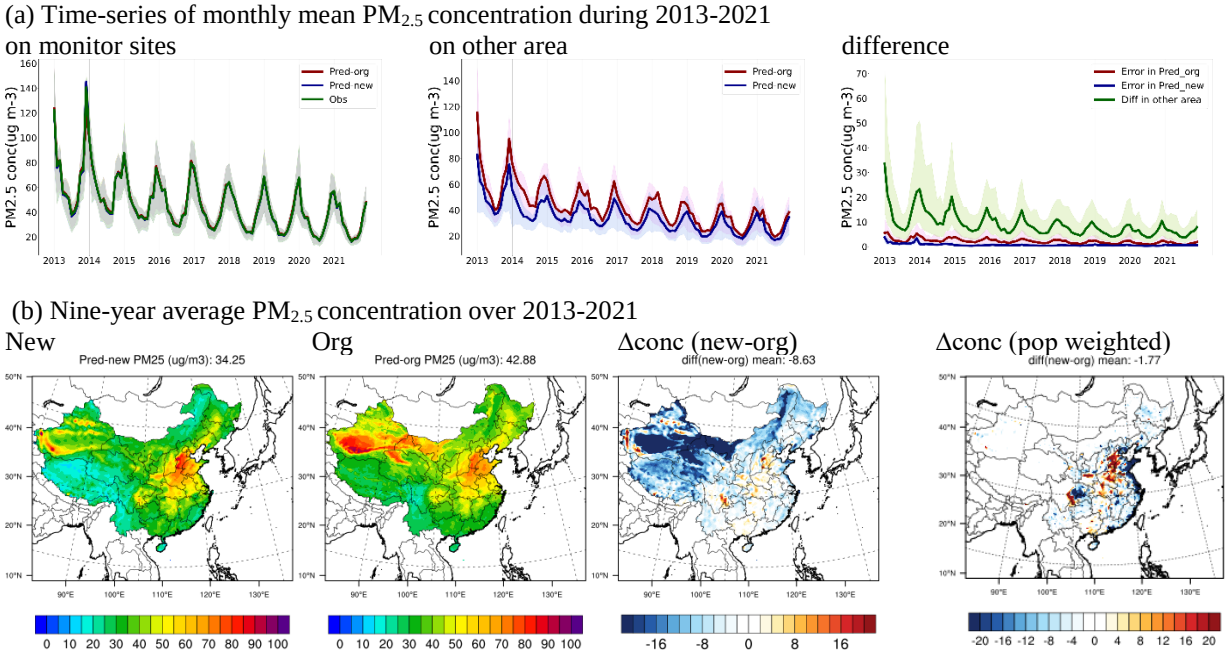

Figure 5: Improve the estimation of $PM_{2.5}$ and related exposure across China with satellite product and ground observations during 2013-2021 (*suburban/rural represent the area within 5 grid cells distance to the monitor sites; results are comparing the ResNet-time model with the baseline RF)

https://doi.org/10.5194/essd-2024-170
Preprint. Discussion started: 15 May 2024

References

Appel, K. W. et al., 2013. Evaluation of dust and trace metal estimates from the Community Multiscale Air Quality (CMAQ) model version 5.0. Geoscientific Model Development, 6, (4), 883-899.

Bai, K., Li, K., Guo, J., & Chang, N. B. (2022). Multiscale and multisource data fusion for full-coverage PM2. 5 concentration mapping: Can spatial pattern recognition come with modeling accuracy?. ISPRS Journal of Photogrammetry and Remote Sensing, 184, 31-44.

Belgiu, M., & Drăguţ, L. (2016). Random forest in remote sensing: A review of applications and future directions. ISPRS journal of photogrammetry and remote sensing, 114, 24-31.

Bellouin, N., Boucher, O., Haywood, J., & Reddy, M. S. (2005). Global estimate of aerosol direct radiative forcing from satellite measurements. Nature, 438(7071), 1138-1141.

Celarier, E. A., Brinksma, E. J., Gleason, J. F., Veefkind, J. P., Cede, A., Herman, J. R., ... & Levelt, P. F. (2008). Validation of Ozone Monitoring Instrument nitrogen dioxide columns. Journal of Geophysical Research: Atmospheres, 113(D15)

Chen, D., Guo, H., Gu, X., Cheng, T., Yang, J., Zhan, Y., & Wei, X. (2023). A spatial-neighborhood deep neural network model for PM 2.5 estimation across China. IEEE Transactions on Geoscience and Remote Sensing.

Chen, T., & Guestrin, C. (2016). Xgboost: A scalable tree boosting system. In Proceedings of the 22nd acm sigkdd international conference on knowledge discovery and data mining (pp. 785-794).

Ding, D., Xing, J., Wang, S., Chang, X., Hao, J., 2019a. Impacts of emissions and meteorological changes on China's ozone pollution in the warm seasons of 2013 and 2017. Frontiers of Environmental Science & Engineering, 13(5), 1-9.

Ding, D.; Xing, J.; Wang, S.; Liu, K.; Hao, J., 2019b. Estimated Contributions of Emissions Controls, Meteorological Factors, Population Growth, and Changes in Baseline Mortality to Reductions in Ambient PM2.5 and PM2.5 -Related Mortality in China, 2013-2017., Environ Health Perspect., 127(6):67009.

Ding, Y., Li, S., Xing, J., Li, X., Ma, X., Song, G., ... & Meng, S. (2024). Retrieving hourly seamless PM2. 5 concentration across China with physically informed spatiotemporal connection. Remote Sensing of Environment, 301, 113901.

Geng, G., Zheng, Y., Zhang, Q., Xue, T., Zhao, H., Tong, D., ... & Davis, S. J. (2021). Drivers of PM2. 5 air pollution deaths in China 2002–2017. Nature Geoscience, 14(9), 645-650.

Guenther, A.B., Jiang, X., Heald, C.L., Sakulyanontvittaya, T., Duhl, T., Emmons, L.K., Wang, X., 2012. The Model of Emissions of gases and Aerosols from Nature version 2.1 (MEGAN2. 1): an extended and updated framework for modeling biogenic emissions. Geosci. Model Dev. 5 (6), 1471–1492

He, K., Zhang, X., Ren, S., & Sun, J. (2016). Deep residual learning for image recognition. In Proceedings of the IEEE conference on computer vision and pattern recognition (pp. 770-778).

Hoff, R. M., & Christopher, S. A. (2009). Remote sensing of particulate pollution from space: have we reached the promised land?. Journal of the Air & Waste Management Association, 59(6), 645-675.

https://doi.org/10.5194/essd-2024-170
Preprint. Discussion started: 15 May 2024

Hu, X., Belle, J. H., Meng, X., Wildani, A., Waller, L. A., Strickland, M. J., & Liu, Y. (2017). Estimating PM2. 5 concentrations in the conterminous United States using the random forest approach. Environmental science & technology, 51(12), 6936-6944.

Ke, G., Meng, Q., Finley, T., Wang, T., Chen, W., Ma, W., ... & Liu, T. Y. (2017). Lightgbm: A highly efficient gradient boosting decision tree. Advances in neural information processing systems, 30.

Kingma, D. P., & Ba, J. (2014). Adam: A method for stochastic optimization. arXiv preprint arXiv:1412.6980.

Kong, L., Tang, X., Zhu, J., Wang, Z., Li, J., Wu, H., ... & Carmichael, G. R. (2021). A 6-year-long (2013–2018) high-resolution air quality reanalysis dataset in China based on the assimilation of surface observations from CNEMC. Earth System Science Data, 13(2), 529-570.

Lelieveld, J., Evans, J. S., Fnais, M., Giannadaki, D., & Pozzer, A. (2015). The contribution of outdoor air pollution sources to premature mortality on a global scale. Nature, 525(7569), 367-371..

Li, T., Shen, H., Yuan, Q., & Zhang, L. (2020). Geographically and temporally weighted neural networks for satellite-based mapping of ground-level PM2. 5. ISPRS Journal of Photogrammetry and Remote Sensing, 167, 178-188.

Liu, X. H., Zhang, Y., Cheng, S. H., Xing, J., Zhang, Q., Streets, D. G., ... & Hao, J. M. (2010). Understanding of regional air pollution over China using CMAQ, part I performance evaluation and seasonal variation. Atmospheric Environment, 44(20), 2415-2426.

Ma, Z., Dey, S., Christopher, S., Liu, R., Bi, J., Balyan, P., & Liu, Y. (2022). A review of statistical methods used for developing large-scale and long-term PM2. 5 models from satellite data. Remote Sensing of Environment, 269, 112827.

Martin, R. V., Jacob, D. J., Chance, K., Kurosu, T. P., Palmer, P. I., & Evans, M. J. (2003). Global inventory of nitrogen oxide emissions constrained by space-based observations of NO2 columns. Journal of Geophysical Research: Atmospheres, 108(D17).

Mitchell, J. F., Johns, T. C., Gregory, J. M., & Tett, S. F. B. (1995). Climate response to increasing levels of greenhouse gases and sulphate aerosols. Nature, 376(6540), 501-504.

Remer, L. A., Kleidman, R. G., Levy, R. C., Kaufman, Y. J., Tanré, D., Mattoo, S., ... & Holben, B. N. (2008). Global aerosol climatology from the MODIS satellite sensors. Journal of Geophysical Research: Atmospheres, 113(D14).

Shin, M., Kang, Y., Park, S., Im, J., Yoo, C., & Quackenbush, L. J. (2020). Estimating ground-level particulate matter concentrations using satellite-based data: A review. GIScience & Remote Sensing, 57(2), 174-189.

Skamarock, W. C., J. B. Klemp, J. Dudhia, D. O. Gill, D. M. Barker, M. G Duda, X.-Y. Huang, W. Wang, and J. G. Powers, A Description of the Advanced Research WRF Version 3. NCAR Tech. Note NCAR/TN-475+STR, 113 pp. 2008.

Teng, M., Li, S., Xing, J., Fan, C., Yang, J., Wang, S., ... & Wang, S. (2023). 72-hour real-time forecasting of ambient PM2. 5 by hybrid graph deep neural network with aggregated neighborhood spatiotemporal information. Environment International, 176, 107971.

https://doi.org/10.5194/essd-2024-170
Preprint. Discussion started: 15 May 2024

Wang, Z., Hu, B., Huang, B., Ma, Z., Biswas, A., Jiang, Y., & Shi, Z. (2022). Predicting annual PM2. 5 in mainland China from 2014 to 2020 using multi temporal satellite product: An improved deep learning approach with spatial generalization ability. ISPRS Journal of Photogrammetry and Remote Sensing, 187, 141-158.

Wang, Z., Li, R., Chen, Z., Yao, Q., Gao, B., Xu, M., ... & Zhou, C. (2022). The estimation of hourly PM2. 5 concentrations across China based on a Spatial and Temporal Weighted Continuous Deep Neural Network (STWC-DNN). ISPRS Journal of Photogrammetry and Remote Sensing, 190, 38-55.

Wei, J., Li, Z., Chen, X., Li, C., Sun, Y., Wang, J., ... & Liu, Y. (2023). Separating Daily 1 km PM2. 5 Inorganic Chemical Composition in China since 2000 via Deep Learning Integrating Ground, Satellite, and Model Data. Environmental science & technology.

Wyat Appel, K., Napelenok, S., Hogrefe, C., Pouliot, G., Foley, K. M., Roselle, S. J., ... & Mathur, R. (2018). Overview and evaluation of the community multiscale air quality (CMAQ) modeling system version 5.2. In Air Pollution Modeling and its Application XXV 35 (pp. 69-73). Springer International Publishing.

Xiao, Q., Chang, H. H., Geng, G., & Liu, Y. (2018). An ensemble machine-learning model to predict historical PM2. 5 concentrations in China from satellite data. Environmental science & technology, 52(22), 13260-13269.

Xing, J., Zheng, S., Ding, D., Kelly, J. T., Wang, S., Li, S., ... & Hao, J. (2020). Deep learning for prediction of the air quality response to emission changes. Environmental science & technology, 54(14), 8589-8600.

Yan, X., Zang, Z., Luo, N., Jiang, Y., & Li, Z. (2020). New interpretable deep learning model to monitor real-time PM2. 5 concentrations from satellite data. Environment international, 144, 106060.

Yarwood, G., Jung, J., Whitten, G. Z., Heo, G., Mellberg, J., & Estes, M. (2010). Updates to the Carbon Bond mechanism for version 6 (CB6). In 9th Annual CMAS Conference, Chapel Hill, NC (pp. 11-13).

Zheng, H. et al., 2019. Transition in source contributions of PM 2.5 exposure and associated premature mortality in China during 2005–2015, Environment International, 475 132.

Zheng, T., Chen, Z., Ding, S., & Luo, J. (2021). Enhancing RF sensing with deep learning: A layered approach. IEEE Communications Magazine, 59(2), 70-76.

Zhong, J., Zhang, X., Gui, K., Wang, Y., Che, H., Shen, X., ... & Zhang, W. (2021). Robust prediction of hourly PM2. 5 from meteorological data using LightGBM. National science review, 8(10), nwaa307.